Acta Geochim (2026) 45:298–313
https://doi.org/10.1007/s11631-025-00810-w

ORIGINAL ARTICLE

Sources and transportation of mining metals to soil: A case study from the Lala mining area, Southwest China

Fang Yang[1,2] · Lei Xu[2] · Liang Tang[2] · Li Dai[3] · Xuemin Liu[2] · Tim T. Werner[4] · Lingfei Qu[5] · Xuefeng Liao[6] · Yang Li[5] · Junbo Wang[7]

Received: 10 May 2025 / Revised: 10 June 2025 / Accepted: 9 July 2025 / Published online: 18 August 2025
© The Author(s), under exclusive licence to Science Press and Institute of Geochemistry, CAS and Springer-Verlag GmbH Germany, part of Springer Nature 2025

Abstract Soil contamination with toxic metals from mining activities poses a risk to ecological security and human well-being, but research on their transport mechanisms is inadequate. Addressing this, this study combines the PCA-APCS-MLR model, hydrological and soil profile analyses, and geographic detector techniques within the Lala mining area, Sichuan Province, China, to explore the connection between soil metal enrichment and mining activities and to assess soil contamination. We identified three primary sources of metals in soils: geogenic background, mining activities, and industrial emissions. Mining activities are the primary source for Mn (13.6%), Cu (33.9%), Mo (69.1%), and As (40.0%) in soil, while industrial inputs contribute to Pb (63.8%), Zn (67.4%), and Cd (83.6%). Meanwhile, dry and wet deposition drove the dispersal mode of mine metals to the soil in the study area. Specifically, coarse mine wastes primarily settle around the mine sites, whereas fine particulates are carried northward by prevailing southwest winds, leading to northward and long-range transport. Our findings are important for assessing the mining industry's footprint in arid environments.

Keywords Heavy metals · Lala mining area · Arable soil · PCA-APCS-MLR model · Mine waste diffusion

1 Introduction

Widespread contamination in arable soils by toxic metals poses a significant challenge to food security and human survival (Cai et al. 2019; Zhang et al. 2023b). Metals in soils can originate from bedrock and anthropogenic activities, such as mining, industrial emissions, and sewage irrigation (Liu et al. 2020b; Long et al. 2021; Xu et al. 2023). The impact of mining on soil quality is a growing environmental concern, particularly in resource-rich industrializing economies with weaker environmental regulations. In China, the massive consumption of mineral resources in recent decades has triggered a surge in pollution incidents, particularly from continuous and extensive open-pit mines (Cheng et al. 2020; Liu et al. 2020b; Ran et al. 2021; Zhou et al. 2024a). An

Fang Yang and Lei Xu have contributed equally to this work.

Supplementary Information The online version contains supplementary material available at https://doi.org/10.1007/s11631-025-00810-w.

✉ Liang Tang
tangliang17@cdut.edu.cn

Li Dai
daili1988517@126.com

[1] Research Center for Planetary Science, Chengdu University of Technology, Chengdu 610059, China

[2] College of Earth and Planetary Sciences, Chengdu University of Technology, Chengdu 610059, China

[3] Institute of Multipurpose Utilization of Mineral Resources, Chinese Academy of Geological Sciences, Chengdu 610041, China

[4] School of Geography, Earth and Atmospheric Sciences, Faculty of Science, The University of Melbourne, Melbourne, Australia

[5] Sichuan Development Environmental Science and Technology Research Institute Co., Ltd., Chengdu 610041, China

[6] Zhongke Yirong Ecological Environment Co., Ltd., Chengdu 610095, China

[7] School of Environment, Tsinghua University, Beijing 100084, China

estimated 1.5 million hectares of land have already been contaminated by mining activities, with the affected area expanding at an alarming rate of 46,700 hectares annually (Xiao et al. 2017).

Toxic metals significantly threaten soil quality due to their persistence and bioaccumulation potential. Consequently, identifying the dispersion mechanisms and pathways is crucial for further mitigating soil metal contamination. Past studies have found that the transportation and redistribution of metals from mining are governed by a range of factors, notably related to aspects of the pollution sources (Liu et al. 2020b; Long et al. 2021; Ran et al. 2021), the receiving environment (Qiao et al. 2023; Yang et al. 2021), the available transport pathways (Qiao et al. 2023; Qin et al. 2023a), and the prevailing geographical climate (Bai et al. 2024; Liu et al. 2020a; Oubane et al. 2021). For example, elevated levels of Fe and Mn in soils facilitate the adsorption and retention of heavy metals (Chen et al. 2010; Dong et al. 2021), and terrain and soil properties (e.g., texture, organic matter) influence the morphology and distribution of metals (Li et al. 2020; Yuan et al. 2021). Alternatively, winds and rainfall can enhance the dispersion of metals in mining areas, leading to an expanded contamination area in adjacent farmlands (Qin et al. 2023a; Wang et al. 2019).

The overlapping presence of mineral extraction, dense industrial operations, and residential areas spatially complicates the identification of pollutant dispersion pathways (Long et al. 2021; Noori et al. 2021; Zhao et al. 2020). Source apportionment techniques are necessary to determine the relative contributions of each source. Such techniques include Principal Component Analysis (PCA) (Cai et al. 2023; Huang et al. 2015; Šajn et al. 2011), Positive Matrix Factorization (PMF) (Yoon et al. 2023; Zhou et al. 2024a), and UNMIX (Lü et al. 2024; Zhou et al. 2024b). The PMF model incorporates non-negative constraints for data matrix factorization but lacks a definitive method for determining optimal factor numbers and demonstrates high sensitivity to data outliers (Cao et al. 2025; Cheng et al. 2020). The UNMIX model exhibits significant uncertainty in source identification when addressing systems with multiple pollution sources (Zhou et al. 2024b). As a development building on PCA (Thurston and Spengler 1985), the Absolute Principal Component Scores-Multiple Linear Regression (APCS-MLR) model provides a more efficient and precise approach for identifying and quantifying pollution sources of soil metals (Luo et al. 2023).

Mining activities can significantly impact surrounding regions, yet as one moves further from a mine site, the boundaries of contaminated soil become more difficult to delineate. Metal source analyses that integrate uncontaminated soil with contaminated soil can be subject to significant bias (Cai et al. 2023; Liu et al. 2020b; Zhou et al. 2024a). As such, regional zoning is essential for evaluating metal pollution and its dispersion pathways (Long et al. 2021; Teng et al. 2010). However, many geographical attributes can remain unquantifiable (e.g., watersheds, geological strata, and soil types). This limitation has led to an overemphasis on quantifiable variables. Geographic detectors, widely employed in research on pollutant dispersion mechanisms, involve assigning specific values to unquantifiable factors, thereby revealing potential driving forces behind spatial variations in pollutant concentrations (Luo et al. 2019; Qiao et al. 2019; Yang et al. 2021; Zhao et al. 2020).

The Lala mining area in Huili County, Sichuan Province, Southwest China, boasts abundant copper (Cu), iron (Fe), and nickel (Ni) resources. Since 1958, continuous mining and smelting activities have led to contamination of soils, as well as surface and underground water. Historically, research on soil metal pollution in mining areas has focused on identifying pollution sources, assessing ecological impacts, and human health risks (Wei et al. 2023; Xiao et al. 2017), with comparatively limited exploration into dispersion mechanisms. This study utilized high-density sampling, spatial distribution analysis, receptor models, and geographic detector models to investigate mine metals' sources and diffusion mechanisms. Our key objectives were to (1) identify the provenance of metals in the soils of the Lala mining area and (2) analyze the metals' dispersion and migration from mine waste to the surrounding soil. This study provides a quantitative basis for assessing the environmental impacts of mining operations in arid environments and developing ecological management/pollution control responses.

2 Materials and methods

2.1 Study area

The Lala mining area lies in the southern region of Huili County, Sichuan Province, in southwest China (101°54′3″–102°7′16″ E, 26°23′54″–26°24′2″ N, Fig. 1), covering around 556.4 km^2. It is characterized by a geologically diverse stratigraphy, spanning the Proterozoic (Pt_1l, Pt_1t, Pt_1d, Pt_1b, Pt_1xq, Pt_1xt, Pt_2h, Pt_2y, Pt_2l, Pt_2lm^2, Pt_2lm^3, Z_2d, and Z_2g), Mesozoic (T_3bg^2, T_3bg^1, J_2y, J_2x, J_2n, K_1x, and K_2l), and Cenozoic (Q*al* p) eras. This region exhibits complex terrain with higher elevations in the north and southwest; the area descends towards lower elevations in the central region (Fig. 1). The Lala mining area, an annual rainfall of around 800 mm, situated in an dry-hot valley, experiences high evaporation rates, leading to significant water scarcity and classifying it as one of the driest regions in southwestern China (Sun et al. 2024). The annual average temperature is around 20 ℃. The strong winds exceed 9 m/s annually, with a wind

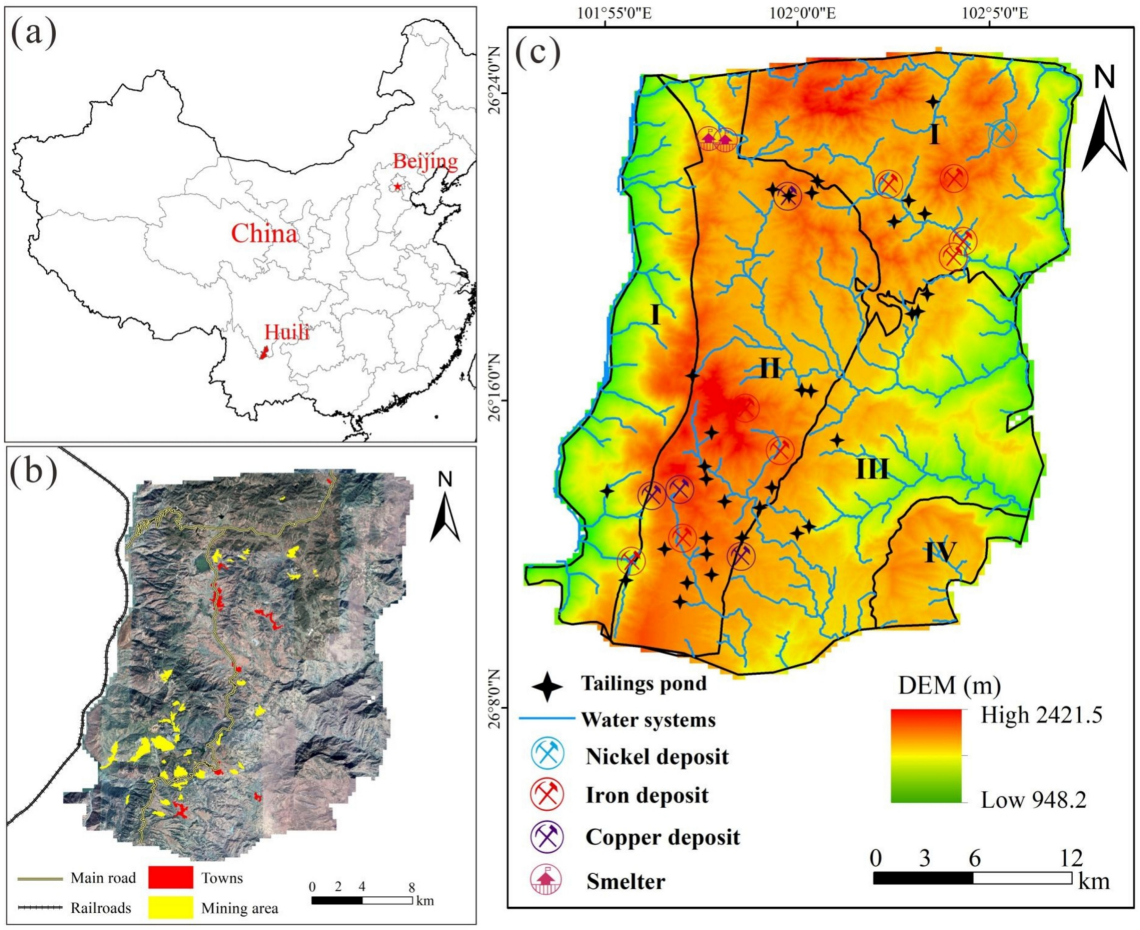


Fig. 1 Overview of the Lala mining area. **a** The location of the Lala mining area in China; **b** Locations of mining areas and key settlement areas; **c** Digital elevation model and distribution of mining activities in the Lala mining area

power density reaching up to 3333.2 kW h/m^2 (Zhong et al. 2017), and prevailing southwest winds (Fig. 2d) (Zhong et al. 2017).

The Lala mining area boasts abundant mineral resources, hosting a large-scale copper mine (Lala Copper Mine), along with three medium-scale mines (Lvshui Copper Mine, Luodong Copper Mine, and Datianaikou Nickel Mine) and nine small-scale mines (Zhou et al. 2019). The Lala Copper Mine (101°57′17″ E, 26°13′30″ N) is located in the southwestern part of the Lala mining area. It is rich in Fe-oxide, Cu-sulfide, and molybdenite (MoS_2), associated with toxic metals, such as rare earth elements, Co, Ni, and U (Song et al. 2020). The operation commenced in 1958 and occupied 0.86 km^2 of land, making it the only regional large-scale mine. Currently, the mining activities are concentrated in the Lala Copper Mine, Lüshui Copper Mine, and four small-scale copper/iron mines. The remaining mines are either suspended or permanently closed. Notably, mining is primarily concentrated in the northeastern and southwestern parts of the study area, surrounded closely by tailings ponds.

2.2 Sampling and measurements

A systematic sampling was conducted to thoroughly investigate the impact of mining on soil. This fieldwork entailed the collection of 1646 soil samples, 75 mining solids samples (ores, slags, and tailings), and 85 surface water samples (Fig. S1, Table S1). The fieldwork adhered to the rigorous technical specifications outlined for soil environmental monitoring (MEE China 2004). Surface soil samples (0–20 cm) were collected from May 2016 to June 2016. Each sample consisted of 3–5 soils spaced 10–20 m apart, and the original weight of the samples was greater than 1 kg to ensure the representativeness of the soil. Soil samples were dried in daylight and gently tapped with a rubber mallet. The samples were then dried and sieved through a nylon sieve, and 500 g of samples of 20 mesh grain size were intercepted for subsequent experiments. Ore, tailings, and waste rock

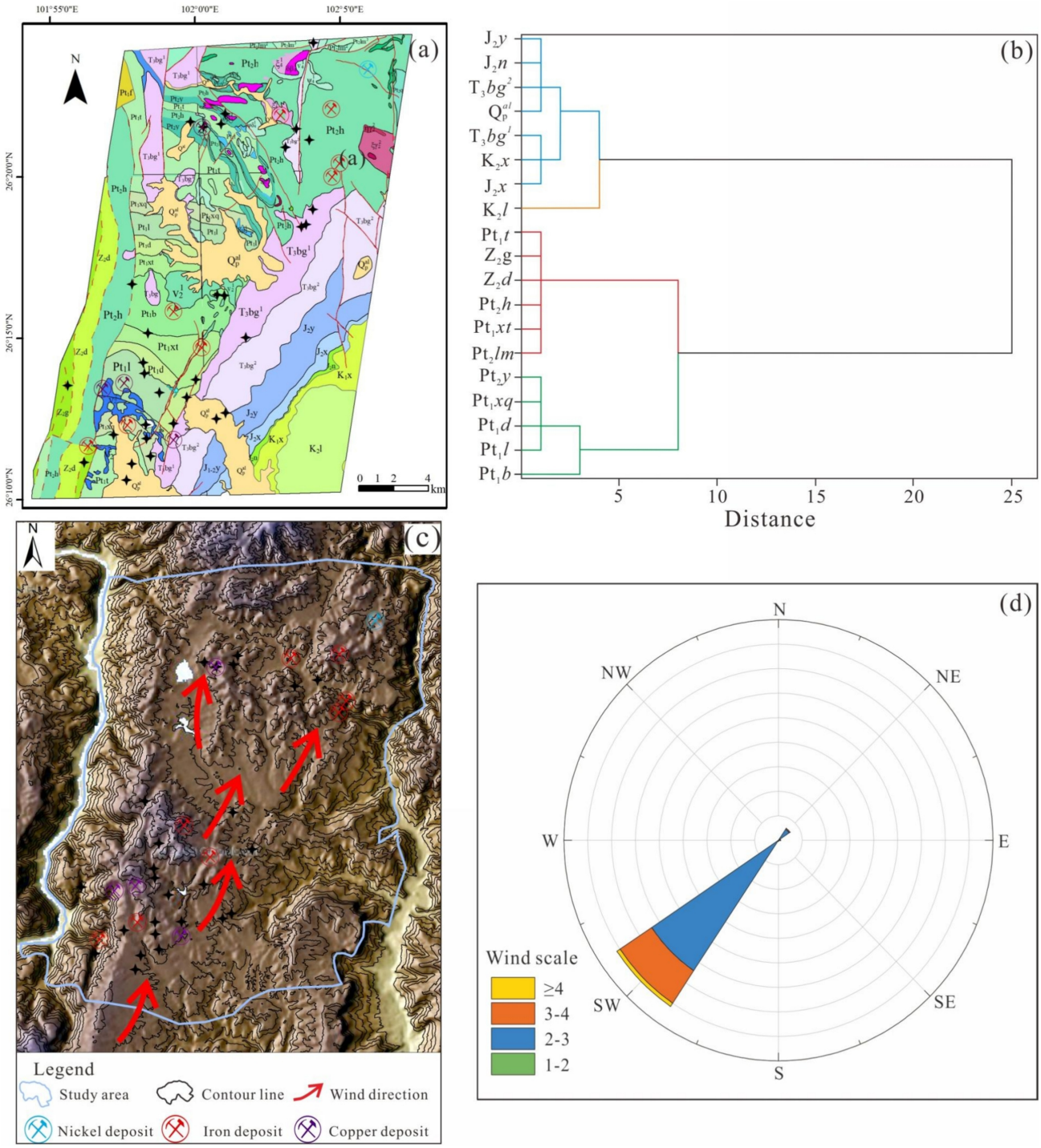


Fig. 2 Geographic attributes of the Lala mining area. **a** Regional geological map of the Lala mining area; **b** The Q-type cluster analysis of stratum; **c** Topographic map and wind direction; **d** The wind rose diagram (date: March 2023–February 2024, and the data originates from historical weather records of Huili County (Weather 2024)

samples were collected in quantities greater than 1.5 kg one by one from mines and tailings ponds. A portable GPS recorded the geographic coordinates of all samples. All samples were analyzed following the outlined protocols (MEE China 2022; MEE and SAMR 2018).

2.3 Statistics

The Q-type cluster analysis employs metal contents constrained by geological strata as variables and integrates geographic location and mine types to segment the Lala

mining area into four distinct zones: Zones I, II, III, and IV (Figs. 1c and 2b). Subsequently, we employed PCA to extract principal components with eigenvalues larger than 1 to identify latent variables influencing soil metal concentrations (Wei et al. 2023). Correlation was analyzed using Kaiser–Meyer–Olkin (KMO) and Bartlett's sphericity tests and normalized using a correlation matrix (Ran et al. 2021). Besides, using the measured metal concentrations, assessment indicator values as dependent variables, and the APCS values as independent variables, we employed the APCS-MLR receptor model to quantify the sources of soil metals (Chen et al. 2022; Yu et al. 2022).

The spatial distribution of soils was visualized using Kriging interpolation in Geographic Information Systems (GIS) to detect the hotspots of heavy metal pollution. Accordingly, hydrologic analysis in GIS was used to simulate runoff and to fit the calculations from the APCS-MLR model.

3 Results

3.1 Soil metal levels and spatial distributions

The geochemical characteristics and spatial distribution of soil metals in the Lala mining area vary greatly. Notably, soil pH varies from 4.29 to 9.44 (mean 5.73), exhibiting a zonal distribution, i.e., acidic soil present in Zones I, II, and III, and alkaline soil prevalent in Zone IV. The abnormally acidic soil is concentrated around mine sites and tailings ponds. The soil contents of TFe, Cu, Co, Mo, and Mn range from 1.40 to 215 g/kg, 7.9 to 2190 mg/kg, 4.06 to 232 mg/kg, 0.10 to 28.5 mg/kg, and 20.0 to 7820 mg/kg, respectively, significantly higher than the established background in Sichuan Province (Wei et al. 1990). Meanwhile, these metals consistently exhibit a northeast-southwest oriented strip distribution, correlating with the outcropping Proterozoic strata in Zones I and II.

The Cr and Ni levels in soil exhibit a wide range, spanning 6.00 to 3130 mg/kg and 4.96 to 1670 mg/kg, respectively. Areas with exceptionally high concentrations form a northeast-southwest-oriented zone in the central low-lying agricultural region and the northeastern mining districts. Soil Zn contents fluctuate between 2.50 and 1500 mg/kg, and As levels range from 0.63 to 516 mg/kg, with outlier points solely found in the northeastern part of the study area. Additionally, Cd and Pb exhibit a wider distribution throughout the soil, with concentrations spanning 0.020 to 4.13 mg/kg and 1.50 to 399 mg/kg, respectively. Anomalous concentrations of these metals are primarily located in the northern region, coinciding with smelting activities (Table 1 and Fig. 3).

Zones I and II probably demonstrate an elevated soil metal level from mining activities. Specifically, Zone I contains elevated Zn, Cr, Ni, and As levels, whereas Zone II displays higher Mn, Cu, and Co concentrations. Meanwhile, the composition of Cu, Mn, Co, and Mo in Zones I and II are higher than the established background levels of Sichuan Province, while Zones III and IV display a composition approaching the background level (Wei et al. 1990). The Coefficient of Variation (CV) serves as a metric to evaluate the impact of human activities on the enrichment of soil metals (Zhang et al. 2021, 2023b). Metal concentrations in Zones I and II displayed significantly higher variability compared to Zones III and IV, with overall CV values exceeding 0.5. Notably, Co, Mn, and Mo exhibited CV values greater than 1, indicating substantial variability (Table 1).

3.2 Geochemical characteristics of ores, slags, and tailings

Collectively, the contents of Cu, Co, Mn, Pb, Zn, Cd, Cr, Ni, Mo, and As in the mining solids (ores, slags, and tailings) range from 17.0 to 15,900 mg/kg, 3.4 to 1190 mg/kg, 267 to 36,600 mg/kg, 3.0 to 2570 mg/kg, 6.96 to 11,700 mg/kg, 0.020 to 6.01 mg/kg, 3.0 to 379 mg/kg, 5.89 to 1280 mg/kg, 0.35 to 3160 mg/kg, and 0.60 to 277 mg/kg, respectively. Notably, the Cu, Co, Mn, and Mo levels in mining solids are significantly higher than those observed in soil. The enrichment of metals in mining solids primarily appears to be influenced by ore elements.

Table 1 depicts the metal levels of mining solids from the zone perspective. Zone I reveals a more significant enrichment of Pb, Zn, Cd, Mo, and As, whereas Cu and Mn are more abundant in Zone II, which is consistent with the distribution of metals in the soil. This evidence implies a potential link between ore types and the metal accumulation in the soil. Zone I is characterized by nickel and iron ore, and Zone II is dominated by copper ore (Table 1).

4 Discussion

4.1 Provenance of soil metals

The PCA was conducted separately from Zones I to IV to monitor the variations in metal sources observed between the southern and northern regions. Prior to PCA, the metals of the four Zones were subjected to KMO and Bartlett tests, yielding values of 0.61 ($p < 0.001$), 0.55 ($p < 0.001$), 0.74 ($p < 0.001$), and 0.84 ($p < 0.001$), from Zones I to IV respectively. The results reveal that Zones I, II, and III contain four principal components with eigenvalues exceeding 1, explaining cumulative variances of 71.5%, 67.5%, and 79.3%,

Table 1 Geochemical statistics of soil, ore, slag, and tailings from the four Zones

Zones		Soil					Ores		Slags			Tailings		
		I	II	III	IV	Background[a]	I	II	I	II	III	I	II	III
TFe (g/kg)	Max	215	191	158	61.0	3.30	350	181	365	122	136	307	296	97.5
	Min	1.40	15.7	10.5	17.8		85.9	47.3	44.5	24.6	73.7	38.8	13.3	77.5
	Mean	67.0	82.3	45.8	36.7		270	117	110	80.9	106	135	111	86.3
	CV	0.40	0.32	0.35	0.24		0.46	0.39	0.62	0.33	0.24	0.71	0.60	0.12
Mn (mg/kg)	Max	7820	7820	4900	760	657	36,600	5550	10,900	10,900	2840	2140	7710	2560
	Min	23.0	20.0	40.0	79.0		2270	937	267	990	1310	851	1120	1900
	Mean	1011	1207	541	353		12,637	3436	3404	2821	1840	1581	3044	2337
	CV	0.90	0.86	0.75	0.53		1.3	0.58	0.96	0.75	0.37	0.37	0.56	0.16
Cu (mg/kg)	Max	1120	2190	109	54.5	31.1	8390	15,900	2020	10,600	7020	3960	4540	640
	Min	11.5	7.9	9.74	19.3		121	68	17.0	34.1	486	79.7	74.8	239
	Mean	113	141	38.7	35.3		2800	4264	577	1263	2746	1241	810	417
	CV	0.96	1.29	0.43	0.20		1.4	1.6	1.3	1.9	1.1	1.2	1.5	0.49
Pb (mg/kg)	Max	238	399	39.0	21.5	30.9	2460	–	21.4	2570	32.4	2100	17.2	3.95
	Min	4.75	1.50	9.97	10.6		–	–	–	–	–	–	–	–
	Mean	22.7	19.8	24.6	16.2		615	/	12.4	151	8.90	528	2.91	3.31
	CV	0.84	0.87	0.22	0.17		2.0	/	0.71	2.0	1.2	2.0	0.67	/
Zn (mg/kg)	Max	1500	652	129	96.2	86.5	9800	123	117	11,700	203	4920	69.7	38.3
	Min	15.8	2.50	12.6	20.4		8.58	11.1	6.96	11.1	26.4	28.0	14.5	23.8
	Mean	101	79.7	75.1	55.7		2460	46.5	54.4	672	74.6	851	45.0	31.5
	CV	1.1	0.64	0.30	0.33		2.0	0.87	0.87	3.7	1.1	2.3	0.68	0.23
Cr (mg/kg)	Max	3130	1850	353	118	79.0	60.0	43.0	379	149	43.0	83.0	143	64.0
	Min	6.6	6.0	35.4	41.9		13.0	11.0	7.59	3.00	24.0	14.0	5.00	48.0
	Mean	189	143	97.5	82.4		33.3	31.5	75.1	31.0	31.0	45.0	40.0	59.0
	CV	1.5	0.71	0.30	0.18		0.69	0.41	1.7	1.1	0.27	0.54	0.83	0.16
Ni (mg/kg)	Max	1670	358	141	56.2	32.6	161	60.6	80.4	124	83.1	147	1280	40.3
	Min	5.86	4.90	9.48	10.2		5.89	20.3	28.2	5.93	43.7	36.2	10.1	12.6
	Mean	82.6	63.1	41.1	30.0		77.7	40.6	52.1	44.4	55.7	70.2	88.8	29.1
	CV	1.6	0.51	0.36	0.32		0.91	0.46	0.40	0.70	0.33	0.57	3.1	0.50
Co (mg/kg)	Max	232	96.8	53.0	22.6	17.6	693	155	440	203	99.3	1190	145	104
	Min	4.06	5.16	4.46	5.06		5.48	16.1	12.3	3.40	45.5	30.8	5.78	46.5
	Mean	31.0	36.8	16.4	12.7		195.7	67.1	88.2	87.6	71.1	252	61.2	68.4
	CV	0.63	0.42	0.34	0.28		1.7	0.80	1.6	1.7	0.34	1.8	0.66	0.46
Cd (mg/kg)	Max	1.40	4.13	0.771	0.315	0.079	6.01	0.60	0.95	0.83	0.59	2.47	0.20	0.12
	Min	0.020	0.024	0.021	0.029		–	0.02	–	–	0.045	–	–	0.072
	Mean	0.197	0.155	0.17	0.12		1.62	0.24	0.23	0.65	0.19	0.46	0.072	0.11
	CV	0.82	1.16	0.50	0.50		0.59	1.0	1.2	2.5	1.4	1.8	0.80	0.12
Mo (mg/kg)	Max	28.5	48.4	5.07	2.86	1.00	3160	418	118	1370	76.3	1640	128	91.9
	Min	0.10	0.10	0.21	0.424		0.35	3.58	1.36	0.73	2.62	2.43	0.68	5.85
	Mean	2.72	2.29	1.51	0.742		808	138	22.5	115	34.4	291	23.0	60.0
	CV	0.93	1.17	0.70	0.53		1.9	1.5	1.8	2.6	0.93	2.3	1.4	0.79
As (mg/kg)	Max	516	51.4	20.5	7.25	10.4	202	22.5	121	277	58.5	142	82.6	13.9
	Min	1.27	0.63	1.87	2.44		3.75	0.69	0.90	0.60	3.43	1.59	0.87	4.65
	Mean	23.3	8.93	7.84	4.10		79.1	7.16	25.9	18.9	18.1	29.7	9.40	8.84
	CV	1.5	0.62	0.40	0.29		1.2	1.3	1.6	3.0	1.5	1.9	1.9	0.53
pH	Max	9.44	7.11	9.09	8.76	6.60	8.94	9.10	9.31	9.13	9.15	8.91	9.19	8.93
	Min	4.29	2.85	4.35	5.41		8.12	8.12	8.60	7.02	8.79	8.31	7.72	8.80
	Mean	5.73	5.72	6.20	6.77		8.55	8.60	8.92	8.52	8.95	8.75	8.54	8.87
	CV	0.10	0.09	0.18	0.15		0.04	0.04	0.02	0.06	0.02	0.03	0.05	0.00

[a]Wei et al. (1990); –: no detection; /: not valuable

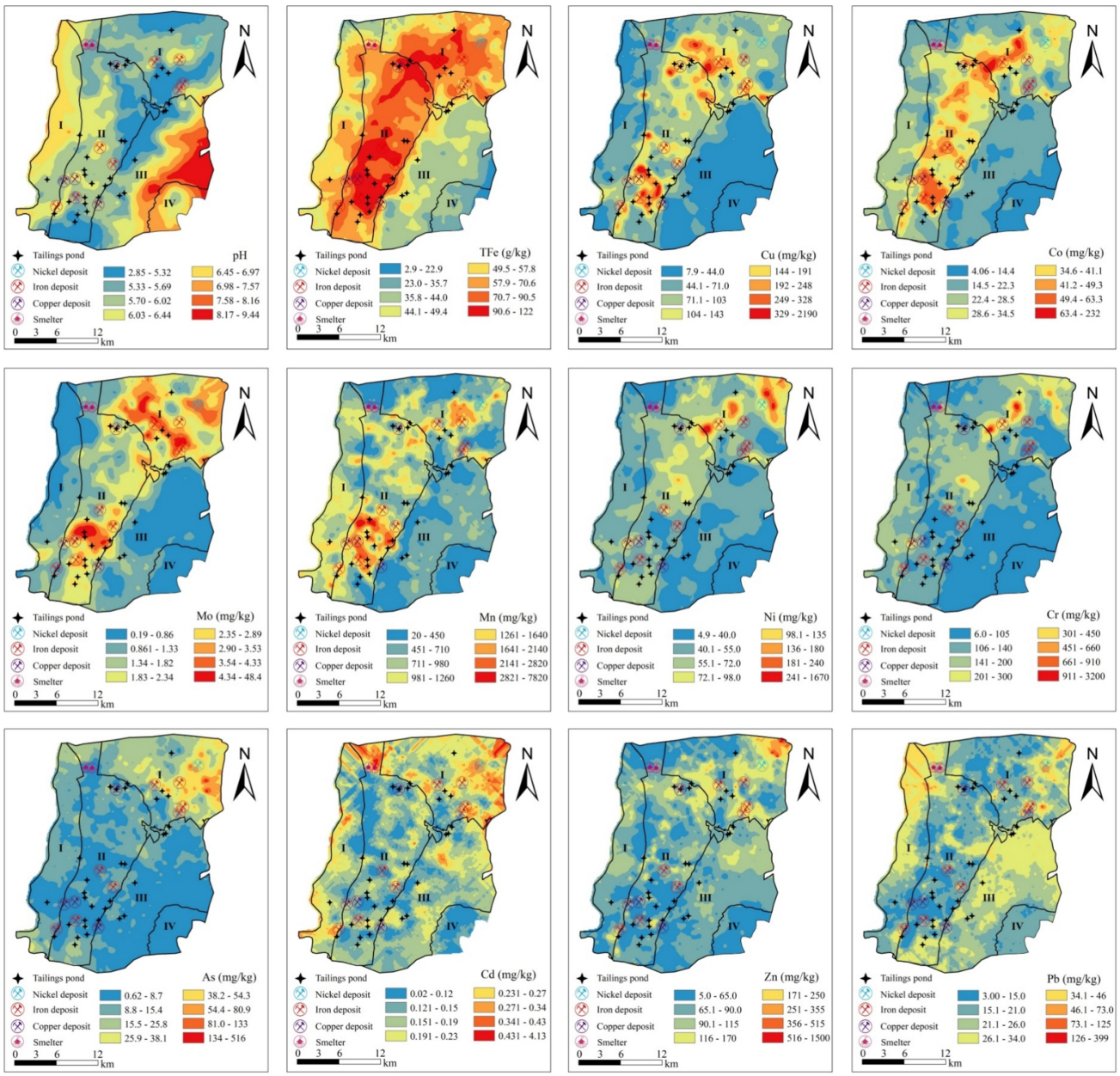


Fig. 3 Spatial distribution of pH and levels of soil metals, Lala mining area

respectively, and two principal components explained 71.4% of the cumulative variances in Zone IV (Table 2).

Metals with high loadings on the same principal component likely originate from a common source (Chen et al. 2022; Lü 2019). Collectively, PC1 exhibits high weights for both Cr and Ni. In the four Zones, there is a significant positive correlation ($r > 0.69$) between Cr and Ni in the soil, indicating a common source (Fig. S2). Additionally, the comparatively lower levels of Cr and Ni in mining solids relative to soil suggest that mining is unlikely to be the primary source of Cr and Ni accumulation (Table 1). It is documented that geogenic Cr and Ni are widely present in pedogenesis processes (Jin et al. 2019; Shi et al. 2022). Therefore, PC1 potentially represents the contribution of natural sources to soil metals.

PC2 reveals higher loadings for TFe, Co, Cu, and Mn (Table 2). Studies have demonstrated that metals (e.g., Cu, Zn, Cr, Ni, Co, Cd, and As) in the Proterozoic strata are at significantly higher levels than those in the Mesozoic and Cenozoic stratum (Zhou et al. 2019). For instance, the estuarine group strata (Pt_2h) within the Proterozoic strata exhibit significant Cu enrichment (Zhou et al. 2019), which is consistent with the higher Cu loadings observed in Zone I. The Fe and Mn are considered constant elements

Table 2 Soil PCA analysis in the Lala mining area on the subdivided Zones perspective

Zones	Factors	TFe	Mn	Cu	Pb	Zn	Cr	Ni	Co	Cd	Mo	As	Eigenvalue	Cumulative variance (%)
I	PC1	− 0.104	0.160	0.206	− 0.078	0.049	0.949	0.934	0.594	0.071	− 0.043	0.040	3.18	71.50
	PC2	0.879	0.456	0.636	− 0.206	0.165	0.117	0.023	0.707	0.009	0.153	0.070	1.41	
	PC3	0.082	− 0.229	0.339	0.461	0.033	− 0.040	0.048	− 0.057	0.165	0.843	0.576	2.06	
	PC4	0.155	0.58	− 0.085	0.599	0.809	0.005	0.099	0.142	0.834	− 0.060	0.265	1.21	
II	PC1	0.038	− 0.117	− 0.001	0.007	0.140	0.909	0.909	0.337	− 0.028	− 0.057	0.166	1.91	67.46
	PC2	0.891	0.491	0.399	− 0.196	0.183	− 0.055	0.157	0.890	0.057	0.101	− 0.450	2.60	
	PC3	0.086	0.212	0.725	0.018	0.015	0.007	− 0.024	0.057	0.012	0.859	0.512	1.26	
	PC4	− 0.005	0.102	0.034	0.804	0.861	− 0.009	0.085	0.020	0.446	− 0.068	0.307	1.66	
III	PC1	0.600	0.209	0.420	0.232	0.492	0.881	0.873	0.743	− 0.103	0.025	0.192	4.78	79.32
	PC2	0.569	0.105	0.698	0.240	− 0.152	0.117	0.175	0.396	0.024	0.846	0.780	1.75	
	PC3	0.301	0.83	0.194	− 0.158	0.149	− 0.045	0.120	0.398	0.419	0.185	− 0.289	1.04	
	PC4	0.000	0.135	0.112	0.813	0.748	0.136	0.251	0.077	0.733	− 0.095	0.254	1.14	
IV	PC1	0.951	0.225	0.877	0.831	0.795	0.893	0.900	0.918	0.07	0.141	0.694	3.194	71.40
	PC4	0.185	0.793	− 0.123	0.166	0.500	0.150	0.308	0.211	0.875	0.750	0.266	1.158	

in chemical weathering and serve as the residues within the epigenetic environment (Zhang et al. 2023a). The soil of the Lala mining area, enriched in Fe/Mn oxides, is predominantly covered by red soil due to the dry-hot valley climate (Mosallaei et al. 2023; Qin et al. 2024). The spatial distribution of Co reveals unusually high concentrations, primarily near mining sites, while moderate levels are mostly associated with the Proterozoic strata. However, Mesozoic and Cenozoic strata generally display noticeably lower Co concentrations (Fig. 3). Meanwhile, the Co/Ni ratio also showed significant variations, reflecting different origins of the parent material in the soil (Zhou et al. 2009). Based on the collective evidence of metal enrichment in Proterozoic strata, spatial distribution, Fe/Mn oxide, and Co/Ni ratios, PC2 can be classified as reflecting the influence of other natural. Therefore, PC1 and PC2 were combined as heavy metals of natural sources.

PC3 displays higher loadings for Cu, Mo, and As, higher loadings in Zones I and II, lower weights in Zone III, and negligible loadings in Zone IV. This distribution pattern closely aligns with the spatial distribution of mine sites within the Lala mining area. Zones I and II experienced prolonged mining of Cu/Fe metals, containing significant amounts of Mo and As as by-products (Song et al. 2020). In Fig. 3, the soil anomalies of Cu, Mo, and As are closely associated with mine sites. Additionally, as described in Sect. 3.2, the Pb, Zn, Cd, Mo, As, Cu and Mn contents in mining solids are closely related to the spatial distribution of metal anomalies in soil. This suggests that PC3 can be attributed to mining activities.

PC4 exhibits high weights for Pb, Zn, and Cd, representing a common source. Notably, the clusters containing Pb, Zn, and Cd differ from the Cr, Ni, and TFe clusters associated with natural sources (Fig. S3). Additionally, the Cd in mining solids is relatively low, comparable to that in soil, suggesting that Cd may not originate from mining activities (Table 1). Likewise, the moderate Pb and Zn levels near mine sites (e.g., Zone I) further weaken the link between these metals and mining. In contrast, Cd is widely found in fossil fuels (Cheng et al. 2018; Elehinafe et al. 2020), and the Lala mining area relies heavily on coke for ores smelting. During coal combustion, Cd preferentially adheres to fine particulate matter, dispersing and settling onto soil (Wen et al. 2020). Furthermore, vehicle wear and consumption of petrol are associated with ore extraction and transportation in the Lala mining area, resulting in Pb and Zn accumulation (Cai et al. 2019; Zhou et al. 2024a). Field investigations in Zone I identified the presence of large-scale smelters and chemical plants that align with the distribution of Pb, Zn, and Cd (Fig. 1). As such, we determine that PC4, indirectly linked to mining, likely represents industrial emissions associated with ore smelting and transportation.

4.2 Quantify sources of soil metals

The PCA-APCS-MLR model was applied to identify and quantify soil metal sources (Luo et al. 2023; Lü 2019). The model's accuracy was evaluated using two metrics: the ratio between predicted and measured values, and the coefficient of determination (R^2) (Luo et al. 2023; Yu et al. 2022; Zhang et al. 2021). The model demonstrated good precision in this study, with a ratio ranging from 0.99 to 1.01 and R^2 varying between 0.20 and 0.94 (Table S2). The lower R^2 of Mn and Cd in Zones I and II probably reflects the uneven distribution caused by mining and industrial emissions.

Figure 4 depicts the relative contributions of various sources to overall soil metal contents. Natural sources emerge as the dominant contributor, followed by mining activities and industrial production. The Lala mining area, abundant in Cu, Fe, and Ni resources, is also accompanied by elevated levels of Mn, Mo, As, and other co-occurring metals, making them the primary contributors to the metal burden in the soils surrounding mine sites (Zeng et al. 2018). Based on the PCA-APCS-MLR model, mining is attributed to the highest proportion to Cu (33.9%), Mo (69.1%), As (40.0%), and a relatively small proportion to Mn (13.6%) in soil. The Mn contamination, although not the primary concern for toxicity, still poses a risk given the unusually high levels found in the soil (Buschmann et al. 2007; McArthur et al. 2012).

Industrial activities emerge as the soil's primary inputs of Pb, Zn, and Cd. Their contribution rates are substantial in Zones I, II, and III, averaging 63.8%, 67.4%, and 83.6%, respectively. Notably, while industrial emissions (e.g., mineral smelting and transportation) contribute less to total soil metal loads than mining, they widely disperse with fine particles, potentially affecting a broader region (Qin et al. 2023a; Yadav et al. 2019).

4.3 Driving forces of metal migration

4.3.1 Southwest prevailing winds

Prevailing winds and monsoons represent an external force that facilitates the long-distance transport of mining dust (Li et al. 2021; Qin et al. 2023a, b). Without disruptive extreme weather events, mining-derived dust typically disperses radially outward from mine sites, creating a circular zone of metal contamination. Given the concentration of mining activity in the southern region, higher metal deposition would be expected in southern soils. However, the spatial distribution of soil metal anomalies exhibits a north–south gradient as observed in Cu, Co, Mo, Ni, As, Cd, and Zn, with a broader extent in the northern regions and a narrower focus in the southern areas (Fig. 3).

Recognizing the predominant role of geological background in soil metal accumulation, this study used offsite contemporary strata in the Lala mining area as a control to isolate geological background impacts on soil metal contents. Prior to comparison, anomalous data points proximal to mining sites were systematically excluded across all strat, as mining-generated coarse particulates primarily settle within adjacent mining areas due to gravitational deposition (Aneja et al. 2012; Patra et al. 2016). The Q^{al}, T_3bg^1, Pt_1xt, and Pt_1d strata exhibited significant regional heterogeneity

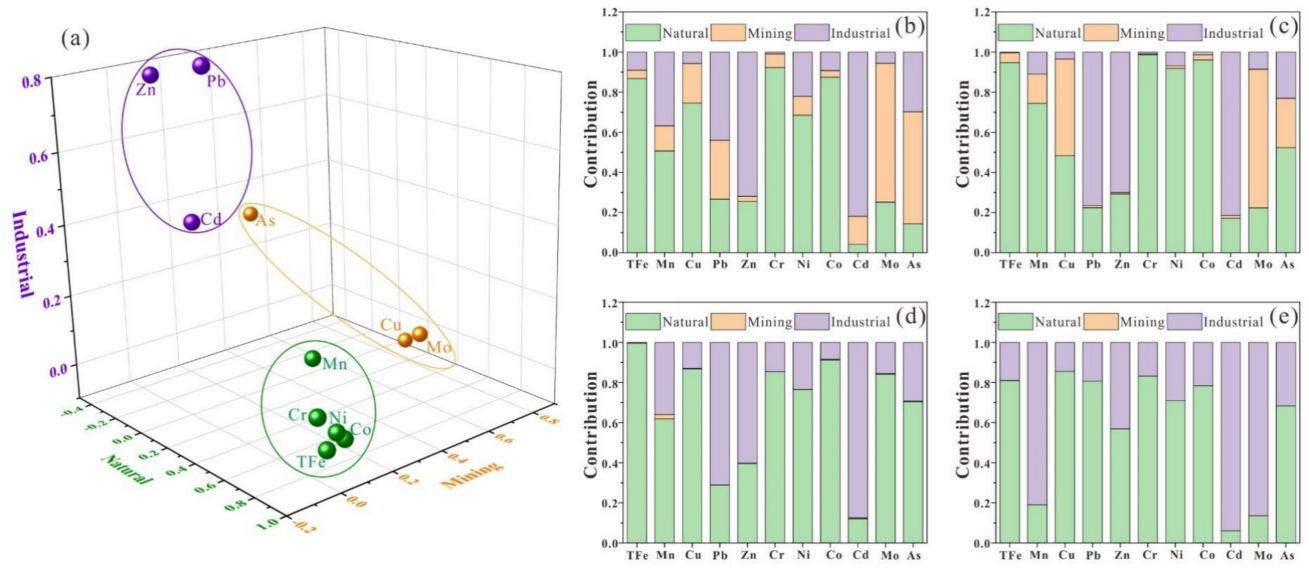


Fig. 4 Source apportionment of metals in soil in the Lala mining area. **a** Results of PCA analyses; Sources apportionment in **b** Zone I, **c** Zone II, **d** Zone III, and **e** Zone IV

in soil metal distribution (Fig. 5), with consistently higher metal concentrations observed in northern strata, particularly for mining-associated Mn, Cu, and Mo (Fig. 5). An exception exists in the Pt_1l stratum, the Pt_1l stratum in the southern region that overlies the copper and iron deposits (Fig. 1c). The Lala mining area's main metallogenic event occurred during the Proterozoic Era (Zeng et al. 2018; Zhu et al. 2017). Consequently, the metal enrichment observed in the Q^{al}, and T_3bg^l strata most accurately reflect mining-related metal dispersion. Within these two strata, northern soils exhibited 30%, 30%, 20%, and 10% higher concentrations of Mn, Cu, Mo, and As, respectively, compared to southern counterparts. This distinct northward enrichment implies that fine mining particulates were likely transported by prevailing southwesterly winds, resulting in enhanced metal accumulation in northern soils.

The deposition of wind-transported contaminants is strongly modulated by topography (An et al. 2023; Li et al. 2022; Qin et al. 2023a). The central Lala mining area features relatively flat terrain, forming a "wind corridor" for southwesterly airflow from the Indian Ocean (Fig. 2c). Windborne particulates preferentially deposit where wind velocity decreases or where topographic barriers occur, leading to enhanced accumulation on high-elevation windward slopes. Six soil profiles with different orientations were established across the study area to quantitatively assess topographic controls on mining-associated metal distribution (Fig. S4). Results demonstrate higher metal concentrations on high-elevation windward slopes versus leeward slopes, particularly near mining zones (Fig. 6).

The Geodetector model was employed to quantify the differential influences of geographic factors (azimuth, and watershed) on metal distribution and identify their driving mechanisms (Wang et al. 2010; Zhao et al. 2020). The decreasing *q*-values for mining-associated metals (Mn, Cu, Mo, and As) with increasing detection distance, indicating progressively weaker explanatory power for directional variations in soil metal concentrations (Fig. 7). The *p*-values also decrease gradually, indicating an increase in confidence because the distant region experiences relatively uniform

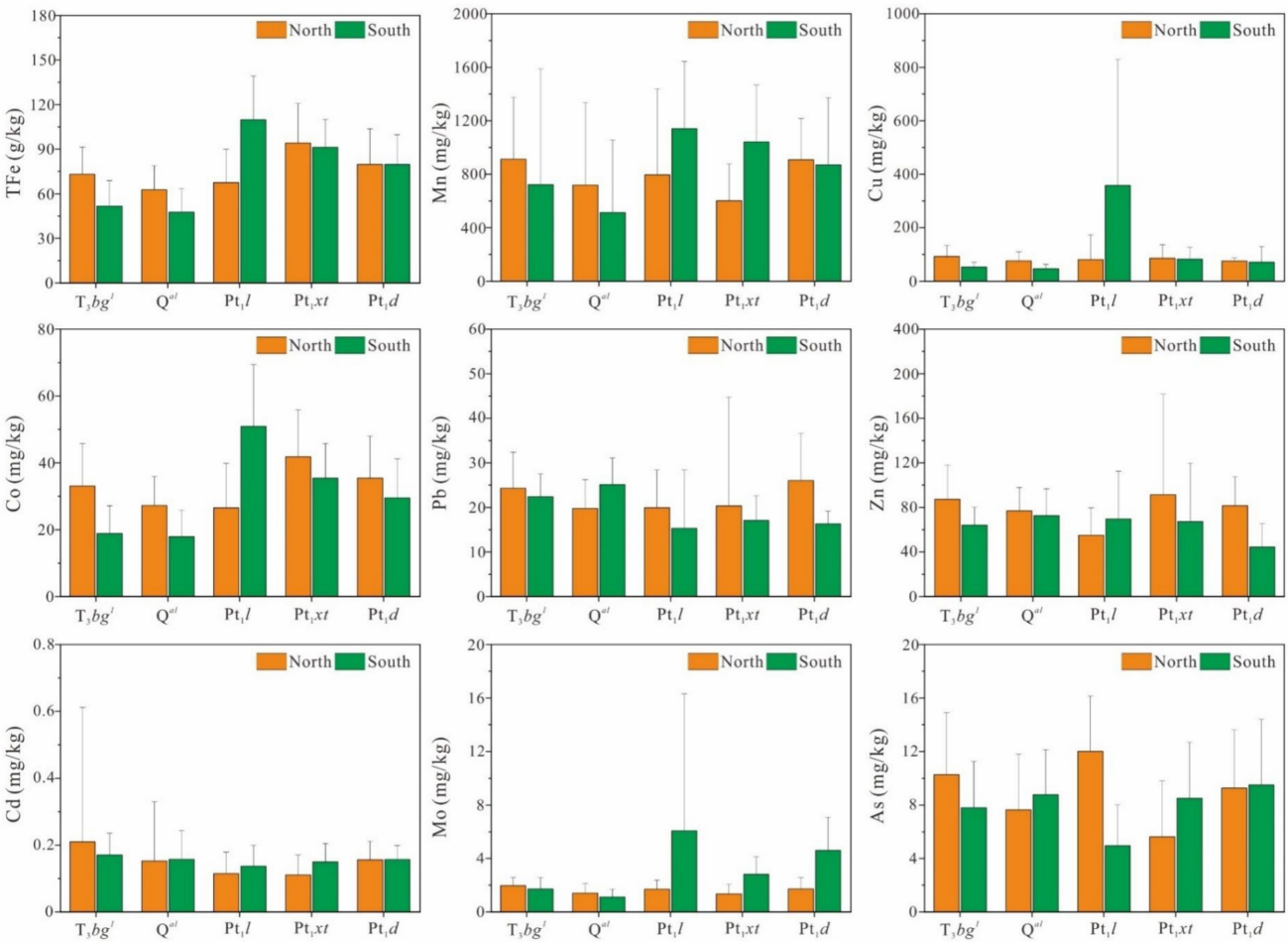


Fig. 5 Soil metal levels in the repetitive strata-constrained perspective in the Lala mining area

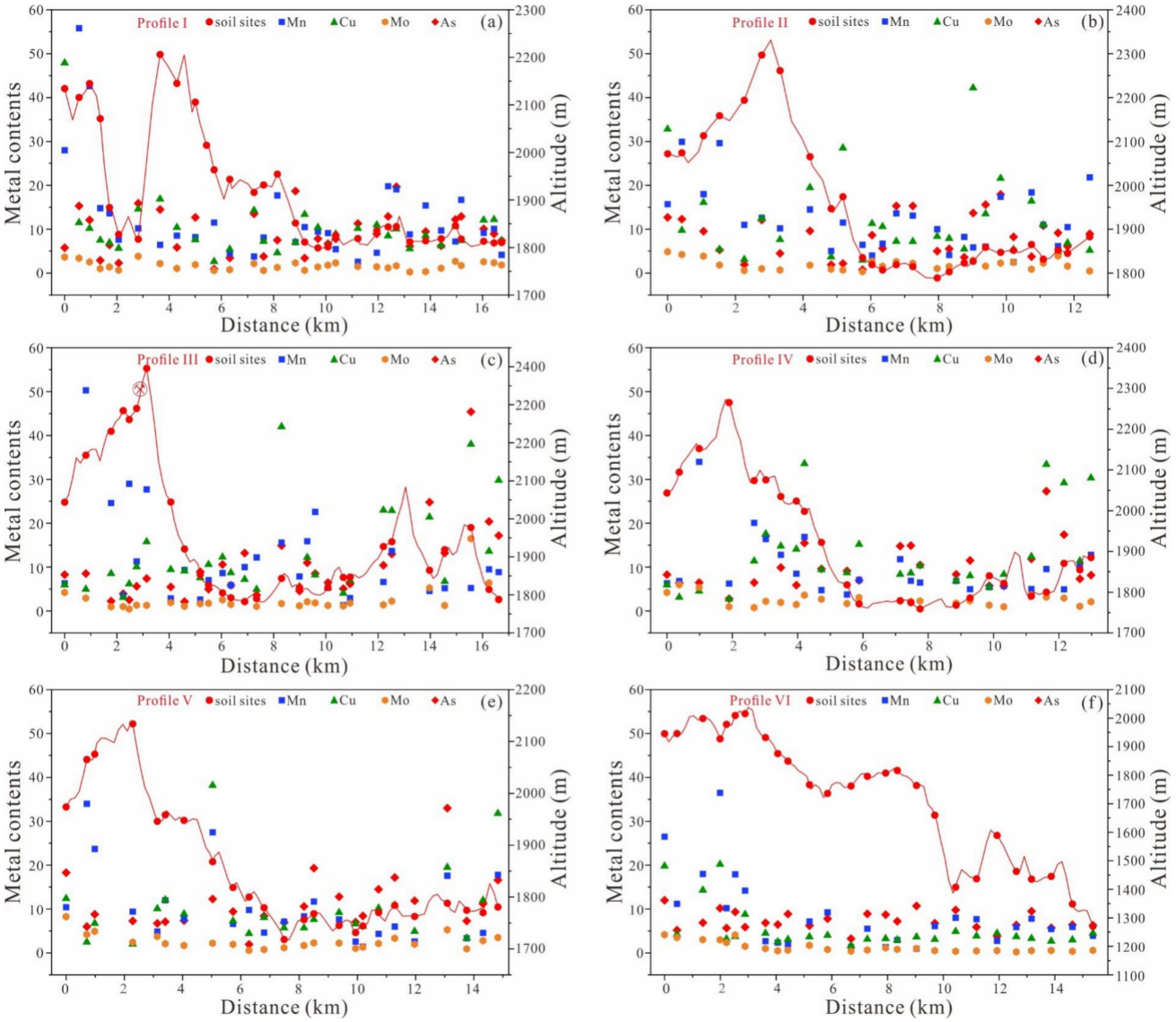


Fig. 6 Metals characteristics along profile lines. The red line represents the profile line; red dots represent the locations of the soil sampling points; the blue squares, green triangles, orange hexagons, and red rhombuses represent the content of Mn (10^2 mg/kg), Cu (10 mg/kg), Mo (mg/kg) and As (mg/kg) under the corresponding soils

directional disturbances (Fig. S6). These trends correspond to the wind propagation, coarse particles preferentially settle near the mine sites and are irrelevant to the wind direction (with higher *q*-values). Alternatively, the fine particles gradually dilute along with the diffusion distance, resulting in lower concentrations (with lower *q*-values) but significantly correlate with azimuth (with lower *p*-values, Fig. S6).

4.3.2 Water-driven

The study area receives annual precipitation > 800 mm, predominantly concentrated during the wet season (typically June to October), which accounts for approximately 85% of the total yearly rainfall (Zhang et al. 2025). Rainfall and runoff represent another critical pathway for metal mobilization (Audoux et al. 2023; Boente et al. 2022). The fitting of Hydrologic analysis and the APCS-MLR model outputs showed significant spatial overlap between mining pollution and the drainage system (Fig. 8). Meanwhile, industrially emitted Pb, Zn, and Cd exhibit analogous deposition (Tian et al. 2020; Zang et al. 2022), corroborating the potential for hydrologic transport of soil metals (Fig. 8).

Fine-scale observational results highlight water-mediated spatial variations in soil metal distribution. In the extensive low altitude farmlands of northeastern Zone I and northern Zone II (Fig. S4), elevated concentrations of

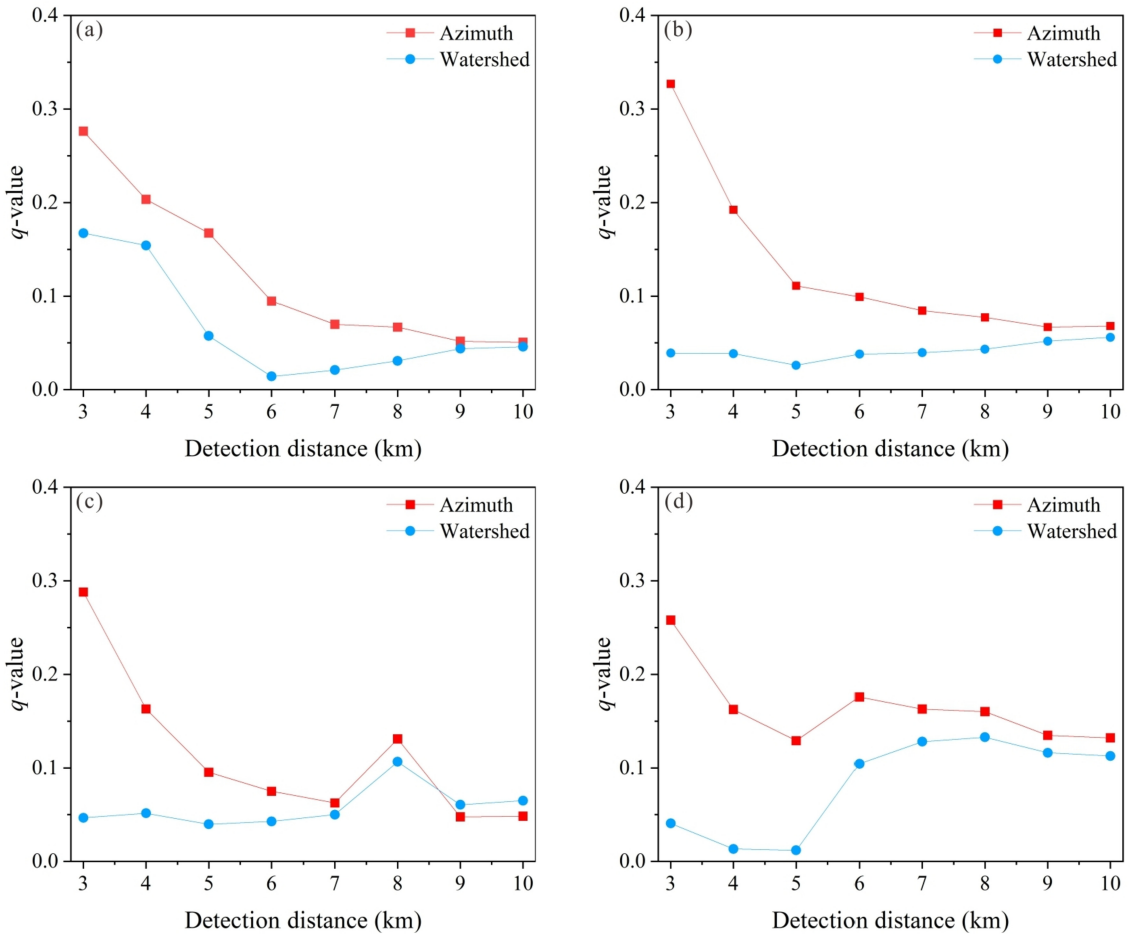


Fig. 7 *q*-values of the independent variables for **a** Mn, **b** Cu, **c** Mo, and **d** As, varying with detection distance. The *q*-value in the factor detection represents the explanation of independent variables on a dependent variable (Wang et al. 2010)

mining-associated metals (Mn, Cu, Mo) show strong correlations with local topography and surface runoff (Fig. 8), suggesting surface water transport as the redistribution mechanism. Meanwhile, localized depressions along the profiles exhibited elevated metal concentrations, indicating hydrologically-driven metal accumulation in these specific areas (Fig. 6). In confirmation, water concentrations of Cu, and total dissolved solid (TDS) proportionally surpass the surface water quality standards (MEE China 2022), even in remote areas from mine sites (Fig. S5).

The spatial heterogeneity of water-driven metals can be further detected through geographical attributes. The explanation metrics (*q*-values) of watersheds for Mn, Cu, Mo, and As exhibited a similar characteristic, which occurs at the 5–6 km mark of the mutation (Fig. 7). Within the 3–5 km interval, the observed decline trends likely correspond to the Jinsha River watershed located on the western side of the study area. As the distance increases, the *q*-values show a decreasing trend. In the range of 5–10 km, it corresponds to watersheds in the central and eastern parts of the study area, and the basin widens and flows away from the Lala copper mine. Consequently, the *q*-values show an increasing trend (Fig. 7). Coincidentally, the straight-line distance from the Lala copper mine to the Jinsha River is approximately 5.5 km. These characteristics demonstrate that precipitation and runoff constitute significant factors influencing the mobilization of mining-derived metals.

5 Conclusions

This study employed PCA-APCS-MLR model to pinpoint the primary sources of metals in soil and quantify their respective contributions to soil concentrations in the Lala mining area. Mining and related industries were primarily responsible for the elevated metal levels in the soil. Cu, Mo, As, Cd, Mn and Zn are contaminated in the study area, of which Cu is strongly contaminated and should be given more attention.

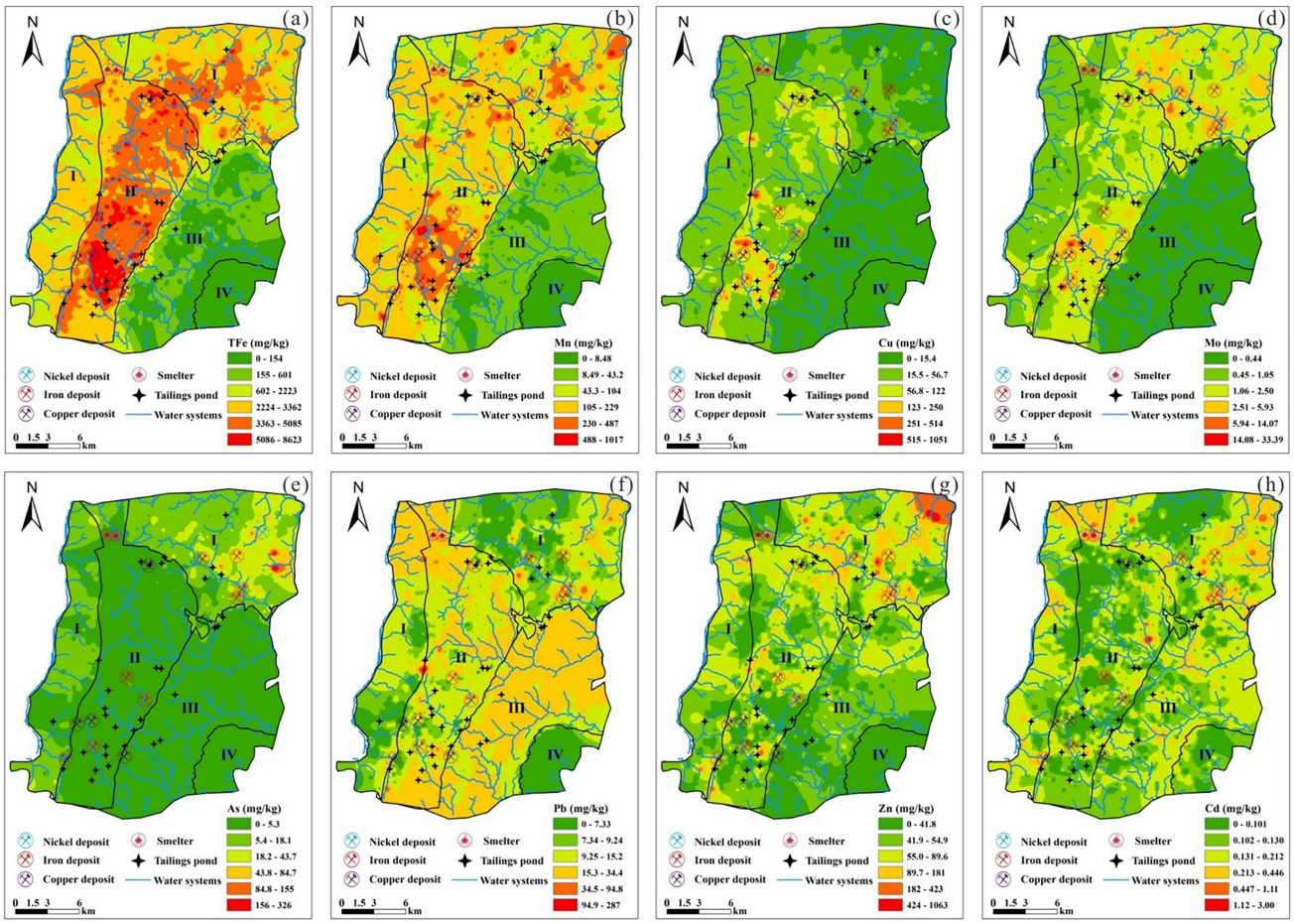


Fig. 8 Distribution of TFe (**a**), Mn (**b**), Cu (**c**), Mo (**d**), and As (**e**) originate from mining and Pb (**f**), Zn (**g**), and Cd (**h**) from industrial emission

The diffusion and migration mechanisms of soil metals were confirmed through hydrological analysis, a geographic detector model, and geological strata comparison. Mining waste is generated from ore extraction, transportation, crushing, and smelting and is primarily settled near the mine sites. Some of these particles are transported by surface runoff to low-lying land. Fine particles, propelled by prevailing southwest wind, steadily migrate northward, depositing in the northern region, leading to a spatial pattern where pollution is higher in the north compared to the south.

Acknowledgements This study was supported by the project "Geological Environment Investigation of the Concentrated Mine Sites of Polymetallic Mineral Resources in Panxi Region, Sichuan Province, China", Nos. DD20160337 and DD20242280, China Geological Survey.

Author contributions FY: Resources, Methodology, Investigation, LX: Methodology, Investigation, Writing—Original Draft, Writing—review and editing; LT: Writing—review and editing, Formal Analysis, Funding Acquisition; LD: Methodology, Investigation, Funding Acquisition; XL: Data Curation, Conceptualization; TTW: Writing—review and editing, Formal Analysis; LQ: Conceptualization; XL: Supervision; YL: Formal Analysis; JW: Methodology.

Funding This work was jointly supported by Geological Environment Investigation of the Concentrated Mine Sites of Polymetallic Mineral Resources in Panxi Region, Sichuan Province (Nos. DD20160337, DD20242280).

Declarations

Conflict of interest The authors declare that they have no conflict of interest.

Ethical approval All authors have approved the manuscript and agree with its submission.

References

An MY, Xing WM, Han YG, Zhou JX, Qu ZX, Zhao CY, Xu P (2023) Analysis and simulation of nitrogen loss during water erosion

process on windward slope under wind-driven rain conditions. CATENA 228:107146. https://doi.org/10.1016/j.catena.2023.107146

Aneja VP, Isherwood A, Morgan P (2012) Characterization of particulate matter (PM10) related to surface coal mining operations in Appalachia. Atmos Environ 54:496–501. https://doi.org/10.1016/j.atmosenv.2012.02.063

Audoux T, Laurent B, Chevaillier S, Féron A, Pangui E, Maisonneuve F, Desboeufs K, Triquet S, Noyalet G, Lauret O, Huet F (2023) Automatic sequential rain sampling to study atmospheric particulate and dissolved wet deposition. Atmos Environ 295:119561. https://doi.org/10.1016/j.atmosenv.2022.119561

Bai ZQ, Li T, Zhang SR, Wang GY, Xu XX, Zhou W, Pan XM, Pu YL, Jia YX, Yang ZB, Long LL (2024) Effects of climate and geochemical properties on the chemical forms of soil Cd, Pb and Cr along a more than 4000 km transect. J Hazard Mater 467:133746. https://doi.org/10.1016/j.jhazmat.2024.133746

Boente C, Millán-Martínez M, Sánchez de la Campa AM, Sánchez-Rodas D, de la Rosa JD (2022) Physicochemical assessment of atmospheric particulate matter emissions during open-pit mining operations in a massive sulphide ore exploitation. Atmos Pollut Res 13(4):101391. https://doi.org/10.1016/j.apr.2022.101391

Buschmann J, Berg M, Stengel C, Sampson ML (2007) Arsenic and manganese contamination of drinking water resources in Cambodia: coincidence of risk areas with low relief topography. Environ Sci Technol 41(7):2146–2152. https://doi.org/10.1021/es062056k

Cai LM, Wang QS, Wen HH, Luo J, Wang S (2019) Heavy metals in agricultural soils from a typical township in Guangdong Province, China: occurrences and spatial distribution. Ecotoxicol Environ Saf 168:184–191. https://doi.org/10.1016/j.ecoenv.2018.10.092

Cai ZQ, Ren BZ, Xie Q, Deng XP, Yin W, Chen LY (2023) Potential toxic heavy metals in village topsoil of antimony mining area: Pollution and distribution, environmental safety: a case study of Qilijiang village in xikuangshan mining area, central Hunan Province, China. Ecol Indic 155:111033. https://doi.org/10.1016/j.ecolind.2023.111033

Cao ZM, Qian H, Gao YY, Li K, Liu YX, Shi XX, Li SQ, Zhao WJ, Yang SH, Tian PP, Wu PX, Ma YD (2025) Ecological risk assessment and source identification of heavy metals in the sediments of the Danjiang River Basin: a quantitative method combining multivariate analysis and the APCS-MLR model. Ecol Indic 175:113518. https://doi.org/10.1016/j.ecolind.2025.113518

Chen GQ, Zeng GM, Du CY, Huang DL, Tang L, Wang L, Shen GL (2010) Transfer of heavy metals from compost to red soil and groundwater under simulated rainfall conditions. J Hazard Mater 181(1–3):211–216. https://doi.org/10.1016/j.jhazmat.2010.04.118

Chen CF, Lim YC, Ju YR, Albarico FPJB, Chen CW, Dong CD (2022) Comparing the applicability of ecological risk indices of metals based on PCA-APCS-MLR receptor models for ports surface sediments. Mar Pollut Bull 185:114361. https://doi.org/10.1016/j.marpolbul.2022.114361

Cheng SW, Liu GJ, Zhou CC, Sun RY (2018) Chemical speciation and risk assessment of cadmium in soils around a typical coal mining area of China. Ecotoxicol Environ Saf 160:67–74. https://doi.org/10.1016/j.ecoenv.2018.05.022

Cheng W, Lei SG, Bian ZF, Zhao YB, Li YC, Gan YD (2020) Geographic distribution of heavy metals and identification of their sources in soils near large, open-pit coal mines using positive matrix factorization. J Hazard Mater 387:121666. https://doi.org/10.1016/j.jhazmat.2019.121666

Dong GW, Han RW, Pan YJ, Zhang CK, Liu Y, Wang HH, Ji XL, Dahlgren RA, Shang X, Chen Z, Zhang MH (2021) Role of MnO_2 in controlling iron and arsenic mobilization from illuminated flooded arsenic-enriched soils. J Hazard Mater 401:123362. https://doi.org/10.1016/j.jhazmat.2020.123362

Elehinafe FB, Mamudu AO, Okedere OB, Ibitioye A (2020) Risk assessment of chromium and cadmium emissions from the consumption of premium motor spirit (PMS) and automotive gas oil (AGO) in Nigeria. Heliyon 6(11):e05301. https://doi.org/10.1016/j.heliyon.2020.e05301

Huang Y, Li TQ, Wu CX, He ZL, Japenga J, Deng MH, Yang XE (2015) An integrated approach to assess heavy metal source apportionment in peri-urban agricultural soils. J Hazard Mater 299:540–549. https://doi.org/10.1016/j.jhazmat.2015.07.041

Jin YL, O'Connor D, Ok YS, Tsang DCW, Liu A, Hou DY (2019) Assessment of sources of heavy metals in soil and dust at children's playgrounds in Beijing using GIS and multivariate statistical analysis. Environ Int 124:320–328. https://doi.org/10.1016/j.envint.2019.01.024

Li JG, Li ZX, Brandis KJ, Bu JW, Sun ZY, Yu Q, Ramp D (2020) Tracing geochemical pollutants in stream water and soil from mining activity in an alpine catchment. Chemosphere 242:125167. https://doi.org/10.1016/j.chemosphere.2019.125167

Li YJ, An XQ, Zhang PQ, Yang JL, Wang C, Li JT (2021) Influence of East Asian winter monsoon on particulate matter pollution in typical regions of China. Atmos Environ 260:118213. https://doi.org/10.1016/j.atmosenv.2021.118213

Li C, Li Y, Fu SM, Jiang XW, Wang XF, Li SS, Cui CG, Hu Y, Cui WJ (2022) A new perspective on the orographic effect of the windward slope on the multi-scale eastward-moving southwest vortex systems. Atmos Res 279:106365. https://doi.org/10.1016/j.atmosres.2022.106365

Liu LH, Ouyang W, Wang YD, Tysklind M, Hao FH, Liu HB, Hao X, Xu YX, Lin CY, Su LY (2020a) Heavy metal accumulation, geochemical fractions, and loadings in two agricultural watersheds with distinct climate conditions. J Hazard Mater 389:122125. https://doi.org/10.1016/j.jhazmat.2020.122125

Liu XY, Shi HD, Bai ZK, Zhou W, Liu K, Wang MH, He YJ (2020b) Heavy metal concentrations of soils near the large opencast coal mine pits in China. Chemosphere 244:125360. https://doi.org/10.1016/j.chemosphere.2019.125360

Long ZJ, Zhu H, Bing HJ, Tian X, Wang ZG, Wang XF, Wu YH (2021) Contamination, sources and health risk of heavy metals in soil and dust from different functional areas in an industrial city of Panzhihua City, Southwest China. J Hazard Mater 420:126638. https://doi.org/10.1016/j.jhazmat.2021.126638

Luo LL, Mei K, Qu LY, Zhang C, Chen H, Wang SY, Di D, Huang H, Wang ZF, Xia F, Dahlgren RA, Zhang MH (2019) Assessment of the Geographical Detector Method for investigating heavy metal source apportionment in an urban watershed of Eastern China. Sci Total Environ 653:714–722. https://doi.org/10.1016/j.scitotenv.2018.10.424

Luo Y, Wang Z, Zhang ZL, Zhang JQ, Zeng QP, Tian D, Li C, Huang FY, Chen S, Chen L (2023) Contamination characteristics and source analysis of potentially toxic elements in dustfall-soil-crop systems near non-ferrous mining areas of Yunnan, southwestern China. Sci Total Environ 882:163575. https://doi.org/10.1016/j.scitotenv.2023.163575

Lü JS (2019) Multivariate receptor models and robust geostatistics to estimate source apportionment of heavy metals in soils. Environ Pollut 244:72–83. https://doi.org/10.1016/j.envpol.2018.09.147

Lü HG, Lu ZH, Fu GX, Lv SF, Jiang J, Xie Y, Luo XH, Zeng JQ, Xue SG (2024) Pollution characteristics and quantitative source apportionment of heavy metals within a zinc smelting site by GIS-based PMF and APCS-MLR models. J Environ Sci 144:100–112. https://doi.org/10.1016/j.jes.2023.09.033

McArthur JM, Sikdar PK, Nath B, Grassineau N, Marshall JD, Banerjee DM (2012) Sedimentological control on Mn, and other trace elements, in groundwater of the Bengal delta. Environ Sci Technol 46(2):669–676. https://doi.org/10.1021/es202673n

MEE China (2004) The technical specification for soil environmental monitoring (HJ/T 166-2004). Standards press of China, Beijing

MEE China (2022) Environmental quality standards for surface water (GB 3838-2022). China Environmental Science Press, Beijing

MEE and SAMR China (2018) Soil environmental quality-Risk control standard for soil contamination of agricultural land (GB15618-2018). China Environmental Science Press, Beijing

Mosallaei S, Abbasi S, Jalalian E, Amiri H, Hoseini M (2023) Heavy metals in edible red soil of the rainbow island in the Persian gulf: concentration and health risk assessment. Chemosphere 331:138778. https://doi.org/10.1016/j.chemosphere.2023.138778

Noori S, Korevaar G, Ramirez AR (2021) Assessing industrial symbiosis potential in emerging industrial clusters: the case of Persian Gulf mining and metal industries special economic zone. J Clean Prod 280:124765. https://doi.org/10.1016/j.jclepro.2020.124765

Oubane M, Khadra A, Ezzariai A, Kouisni L, Hafidi M (2021) Heavy metal accumulation and genotoxic effect of long-term wastewater irrigated peri-urban agricultural soils in semiarid climate. Sci Total Environ 794:148611. https://doi.org/10.1016/j.scitotenv.2021.148611

Patra AK, Gautam S, Kumar P (2016) Emissions and human health impact of particulate matter from surface mining operation: a review. Environ Technol Innov 5:233–249. https://doi.org/10.1016/j.eti.2016.04.002

Qiao PW, Wang S, Li JB, Shan Y, Wei Y, Zhang ZG, Lei M (2023) Quantitative analysis of the contribution of sources, diffusion pathways, and receptor attributes for the spatial distribution of soil heavy metals and their nested structure analysis in China. Sci Total Environ 882:163647. https://doi.org/10.1016/j.scitotenv.2023.163647

Qiao PW, Yang SC, Lei M, Chen TB, Dong N (2019) Quantitative analysis of the factors influencing spatial distribution of soil heavy metals based on geographical detector. Sci Total Environ 664:392–413. https://doi.org/10.1016/j.scitotenv.2019.01.310

Qin MH, Jin YL, Peng TY, Zhao B, Hou DY (2023a) Heavy metal pollution in Mongolian-Manchurian grassland soil and effect of long-range dust transport by wind. Environ Int 177:108019. https://doi.org/10.1016/j.envint.2023.108019

Qin XC, Dong XY, Tao ZH, Wei RF, Zhang H, Guo QJ (2023b) Tracing the transboundary transport of atmospheric Particulate Bound Mercury driven by the East Asian monsoon. J Hazard Mater 446:130678. https://doi.org/10.1016/j.jhazmat.2022.130678

Qin XQ, Guinoiseau D, Ren ZL, Benedetti MF (2024) Redox control of chromium in the red soils from China evidenced by Cr stable isotopes. J Hazard Mater 465:133406. https://doi.org/10.1016/j.jhazmat.2023.133406

Ran HZ, Guo ZH, Yi LW, Xiao XY, Zhang L, Hu ZH, Li CZ, Zhang YX (2021) Pollution characteristics and source identification of soil metal(loid)s at an abandoned arsenic-containing mine, China. J Hazard Mater 413:125382. https://doi.org/10.1016/j.jhazmat.2021.125382

Šajn R, Halamić J, Peh Z, Galović L, Alijagić J (2011) Assessment of the natural and anthropogenic sources of chemical elements in alluvial soils from the Drava River using multivariate statistical methods. J Geochem Explor 110(3):278–289. https://doi.org/10.1016/j.gexplo.2011.06.009

Shi XM, Liu S, Song L, Wu CS, Yang B, Lu HZ, Wang X, Zakari S (2022) Contamination and source-specific risk analysis of soil heavy metals in a typical coal industrial city, Central China. Sci Total Environ 836:155694. https://doi.org/10.1016/j.scitotenv.2022.155694

Song H, Chi GX, Zhang CJ, Xu DR, Xu ZQ, Fan G, Zhang GY (2020) Uranium enrichment in the lala Cu-Fe deposit, Kangdian Region, China: a new case of uranium mineralization associated with an IOCG system. Ore Geol Rev 121:103463. https://doi.org/10.1016/j.oregeorev.2020.103463

Sun L, Sun RH, Chen LD, Sun T, Yang WT, Xin HR, Zeng QH (2024) Larger water use efficiency associated with greater dependence on deep water sources in hot-dry valleys with reservoirs. J Hydrol 630:130756. https://doi.org/10.1016/j.jhydrol.2024.130756

Teng YG, Ni SJ, Wang JS, Zuo R, Yang J (2010) A geochemical survey of trace elements in agricultural and non-agricultural topsoil in Dexing area, China. J Geochem Explor 104(3):118–127. https://doi.org/10.1016/j.gexplo.2010.01.006

Thurston GD, Spengler JD (1985) A quantitative assessment of source contributions to inhalable particulate matter pollution in metropolitan Boston. Atmos Environ 19(1):9–25. https://doi.org/10.1016/0004-6981(85)90132-5

Tian X, Ye AL, He QS, Wang ZT, Guo LL, Chen LG, Liu M, Wang YH (2020) A three-year investigation of metals in the atmospheric wet deposition of a basin region, North China: pollution characteristics and source apportionment. Atmos Pollut Res 11(4):793–802. https://doi.org/10.1016/j.apr.2020.01.007

Wang JF, Li XH, Christakos G, Liao YL, Zhang T, Gu X, Zheng XY (2010) Geographical detectors-based health risk assessment and its application in the neural tube defects study of the Heshun Region, China. Int J Geogr Inf Sci 24(1):107–127. https://doi.org/10.1080/13658810802443457

Wang P, Sun ZH, Hu YA, Cheng HF (2019) Leaching of heavy metals from abandoned mine tailings brought by precipitation and the associated environmental impact. Sci Total Environ 695:133893. https://doi.org/10.1016/j.scitotenv.2019.133893

Weather H (2024) Huili historical weather. https://tianqi.2345.com/wea_history/70722.htm. Accessed 15 Jan 2025

Wei FS, Chen JS, Wu YY, Zheng CJ, Jiang DZ (1990) Background values of soil elements in China. China Environmental Science Press, Beijing

Wei MC, Pan AF, Ma RY, Wang H (2023) Distribution characteristics, source analysis and health risk assessment of heavy metals in farmland soil in Shiquan County, Shaanxi Province. Process Saf Environ Prot 171:225–237. https://doi.org/10.1016/j.psep.2022.12.089

Wen YB, Li W, Yang ZF, Zhang QZ, Ji JF (2020) Enrichment and source identification of Cd and other heavy metals in soils with high geochemical background in the Karst region, Southwestern China. Chemosphere 245:125620. https://doi.org/10.1016/j.chemosphere.2019.125620

Xiao R, Wang S, Li RH, Wang JJ, Zhang ZQ (2017) Soil heavy metal contamination and health risks associated with artisanal gold mining in Tongguan, Shaanxi, China. Ecotoxicol Environ Saf 141:17–24. https://doi.org/10.1016/j.ecoenv.2017.03.002

Xu J, Li YY, Wang SL, Long S, Wu YN, Chen ZM (2023) Sources, transfers and the fate of heavy metals in soil-wheat systems: the case of lead (Pb)/zinc (Zn) smelting region. J Hazard Mater 441:129863. https://doi.org/10.1016/j.jhazmat.2022.129863

Yadav IC, Devi NL, Singh VK, Li J, Zhang G (2019) Spatial distribution, source analysis, and health risk assessment of heavy metals contamination in house dust and surface soil from four major cities of Nepal. Chemosphere 218:1100–1113. https://doi.org/10.1016/j.chemosphere.2018.11.202

Yang X, Yang Y, Wan YY, Wu RJ, Feng DK, Li K (2021) Source identification and comprehensive apportionment of the accumulation of soil heavy metals by integrating pollution landscapes, pathways, and receptors. Sci Total Environ 786:147436. https://doi.org/10.1016/j.scitotenv.2021.147436

Yoon S, Kim DM, Yu S, Park J, Yun ST (2023) Metal(loid)-specific sources and distribution mechanisms of riverside soil contamination near an abandoned gold mine in Mongolia. J Hazard Mater 443:130294. https://doi.org/10.1016/j.jhazmat.2022.130294

Yu L, Zheng TY, Yuan RY, Zheng XL (2022) APCS-MLR model: a convenient and fast method for quantitative identification of nitrate

pollution sources in groundwater. J Environ Manag 314:115101. https://doi.org/10.1016/j.jenvman.2022.115101

Yuan YY, Liu SL, Wu M, Zhong MY, Shahid MZ, Liu YL (2021) Effects of topography and soil properties on the distribution and fractionation of REEs in topsoil: a case study in Sichuan Basin, China. Sci Total Environ 791:148404. https://doi.org/10.1016/j.scitotenv.2021.148404

Zang F, Chang YP, Zhao XN, Wang H, Zhao CY, Nan ZR, Wang SL, Wu Y (2022) Influence of atmospheric trace elements wet deposition on soils and vegetation of Qilian Mountain forests, China. Ecol Indic 141:109151. https://doi.org/10.1016/j.ecolind.2022.109151

Zeng M, Zhang DX, Zhang ZT, Li TX, Li CW, Wei CC (2018) Structural controls on the Lala iron-copper deposit of the Kangdian metallogenic province, southwestern China: tectonic and metallogenic implications. Ore Geol Rev 97:35–54. https://doi.org/10.1016/j.oregeorev.2018.04.028

Zhang YQ, Wang ST, Gao ZJ, Zhang HR, Zhu ZH, Jiang B, Liu JT, Dong HZ (2021) Contamination characteristics, source analysis and health risk assessment of heavy metals in the soil in Shi River Basin in China based on high density sampling. Ecotoxicol Environ Saf 227:112926. https://doi.org/10.1016/j.ecoenv.2021.112926

Zhang XL, Deng YE, Tang L, Hou ZM, Yang JS (2023a) Chemical weathering profile in the V-Ti–Fe mine tailings pond: a basalt-weathering analog. Acta Geochim 42(6):1035–1050. https://doi.org/10.1007/s11631-023-00635-5

Zhang YX, Song B, Zhou ZY (2023b) Pollution assessment and source apportionment of heavy metals in soil from lead–Zinc mining areas of South China. J Environ Chem Eng 11(2):109320. https://doi.org/10.1016/j.jece.2023.109320

Zhang BJ, Zhao X, Dong YF, Xiong DH, Li XY (2025) Morphological characteristics and influencing factors of gully headwall scour holes in Yuanmou Dry-hot Valley region, Southwestern China. CATENA 249:108721. https://doi.org/10.1016/j.catena.2025.108721

Zhao YJ, Deng QY, Lin Q, Zeng CY, Zhong C (2020) Cadmium source identification in soils and high-risk regions predicted by geographical detector method. Environ Pollut 263:114338. https://doi.org/10.1016/j.envpol.2020.114338

Zhong YC, Ma ZF, Guo HY, Deng GW, Xu JX (2017) Analysis of wind energy resources in Huili. Plateau Mt Meteor Res 37(2):72–77 (**in Chinese with English abstract**)

Zhou JY, Mao JW, Zhu ZM, Chen JB, Shen B, Luo LP (2009) Fluid processes in the Lara Iron Oxide-Copper-Gold (IOCG) deposit: trace element constraints on pyrite at different stages of mineralisation. J Min 29(S1):272–273 (**in Chinese**)

Zhou JY, Dai L, Mao YL, Zhang Y, Deng J, Deng B, Zhang J, Luo LP, Yi JC, Zhou JW, Zhu ZX, Sun YJ, Hui B (2019) Concentrated mining area of polymetallic mineral resources in West Panxi Region Report on the Results of Geological and Environmental Investigations. Institute of Comprehensive Utilisation of Minerals, Chinese Academy of Geological Sciences, 132–312 (**in Chinese**)

Zhou H, Yue XM, Chen Y, Liu YZ (2024a) Source-specific probabilistic contamination risk and health risk assessment of soil heavy metals in a typical ancient mining area. Sci Total Environ 906:167772. https://doi.org/10.1016/j.scitotenv.2023.167772

Zhou WT, Yu RY, Guo FH, Shen CY, Liu YJ, Huang YF (2024b) Source apportionment and risk assessment of soil heavy metals in the Huangshui River Basin using a hybrid model. Ecol Indic 160:111906. https://doi.org/10.1016/j.ecolind.2024.111906

Zhu ZM, Tan HQ, Liu YD, Li C (2017) Multiple episodes of mineralization revealed by re-Os molybdenite geochronology in the Lala Fe-Cu deposit, SW China. Miner Deposita 53(3):311–322. https://doi.org/10.1007/s00126-017-0740-x

Publisher's Note Springer Nature remains neutral with regard to jurisdictional claims in published maps and institutional affiliations.

Springer Nature or its licensor (e.g. a society or other partner) holds exclusive rights to this article under a publishing agreement with the author(s) or other rightsholder(s); author self-archiving of the accepted manuscript version of this article is solely governed by the terms of such publishing agreement and applicable law.